Smart Naked-Eye Repeatable off-on-off and on-off-on Switching Luminescent Copper(I)-1H-imidazo[4,5-f][1,10]phenanthroline Complexes with Reversible Acid-Base Responses

Ying Shi, Xia Liu, Yuyu Shan, Weibo Kong, Yuenan Lu, Zhidan Tan, Xiu-Ling Li*

School of Chemistry and Materials Science & Jiangsu Key Laboratory of Green Synthetic Chemistry for Functional Materials, Jiangsu Normal University, Xuzhou, Jiangsu 221116, China

Table S1. Crystallographic data and select refinement details for **1a**, **2b**·$2CH_2Cl_2$·H_2O and **3b**·MeOH·H_2O

	1a	**2b**·$2CH_2Cl_2$·H_2O	**3b**·MeOH·H_2O
Empirical formula	$C_{59}H_{42}CuF_6N_4OP_3$	$C_{64}H_{51}Cl_4CuN_4O_2P_2$	$C_{68}H_{51}CuN_4O_2P_2$
Formula weight	1093.41	1175.36	1081.60
T (K)	150(2)	150(2)	150(2)
Wavelength (Å)	0.71073	0.71073	0.71073
Crystal system	monoclinic	triclinic	triclinic
Space group	$C2/c$	$P\bar{1}$	$P\bar{1}$
Unit cell dimensions			
a (Å)	42.967(2)	11.7392(4)	11.303(4)
b (Å)	11.6599(6)	16.1442(5)	13.704(4)
c (Å)	24.2264(12)	16.9695(6)	21.312(7)
α (°)	90	65.6720(10)	105.655(4)
β (°)	116.906(2)	72.0060(10)	100.773(4)
γ (°)	90	82.8840(10)	101.648(4)
V (Å^3)	10823.5(10)	2787.13(16)	3009.6(16)
Z	8	2	2
D_{calc} (Mg·m^{-3})	1.342	1.401	1.194
μ (mm^{-1})	0.557	0.691	0.462
F(000)	4480	1212	1124
Reflections collected	46417	43145	18224
Independent reflections	12558	14575	13256
Reflections with $I > 2\sigma(I)$	8260	12763	10210
Data/restraints/parameters	12558/1/671	14575/0/705	13256/0/695
Goodness-of-fit (GOF) on F^2	1.023	1.061	1.038
Final R indices [$I > 2\sigma(I)$]	0.0549	0.0386	0.0420
wR_2 [$I > 2\sigma(I)$]	0.1434	0.1112	0.1055
R indices (all data)	0.0901	0.0443	0.0594
wR_2 (all data)	0.1708	0.1150	0.1141

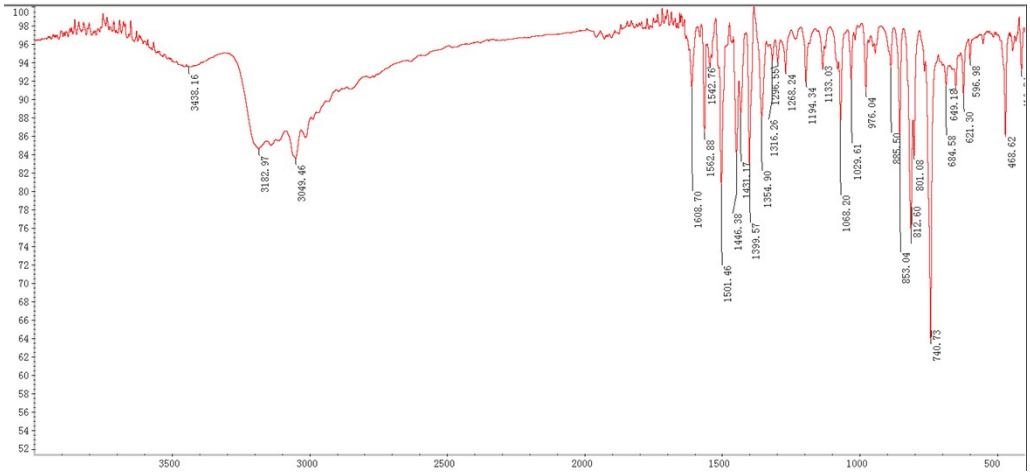

Figure S1. IR spectra of nimpH (*X*-axis: cm⁻¹; *Y*-axis: transmittance).

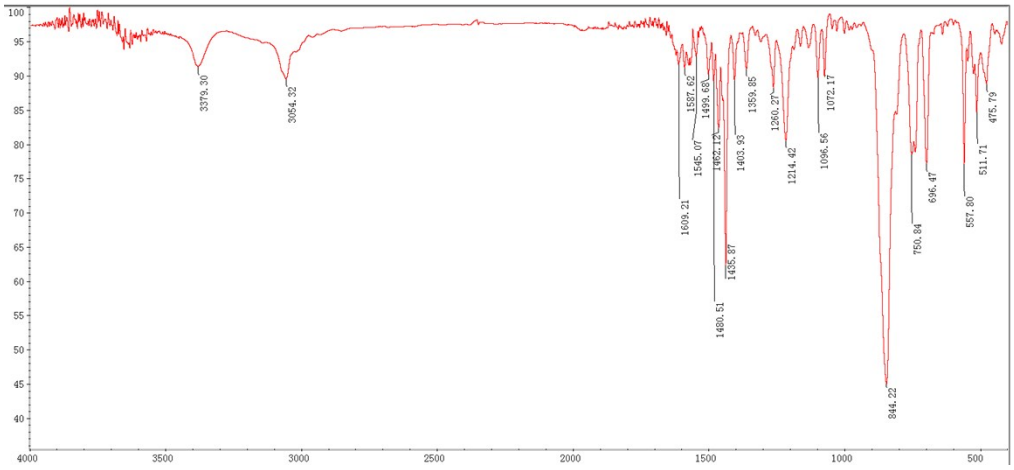

Figure S2. IR spectra of complex **1a**. (*X*-axis: cm⁻¹; *Y*-axis: transmittance).

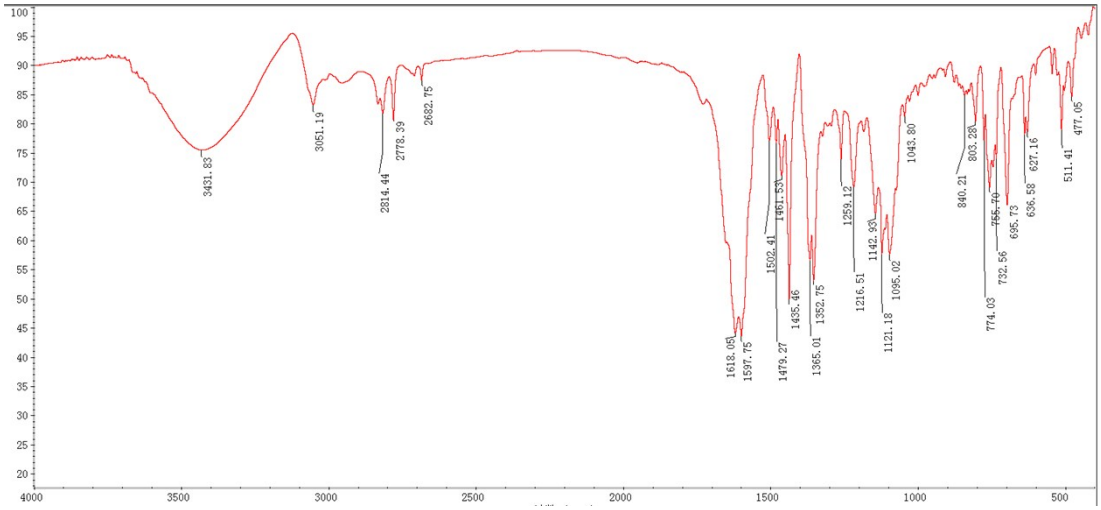

Figure S3. IR spectra of complex **1b**. (*X*-axis: cm⁻¹; *Y*-axis: transmittance).

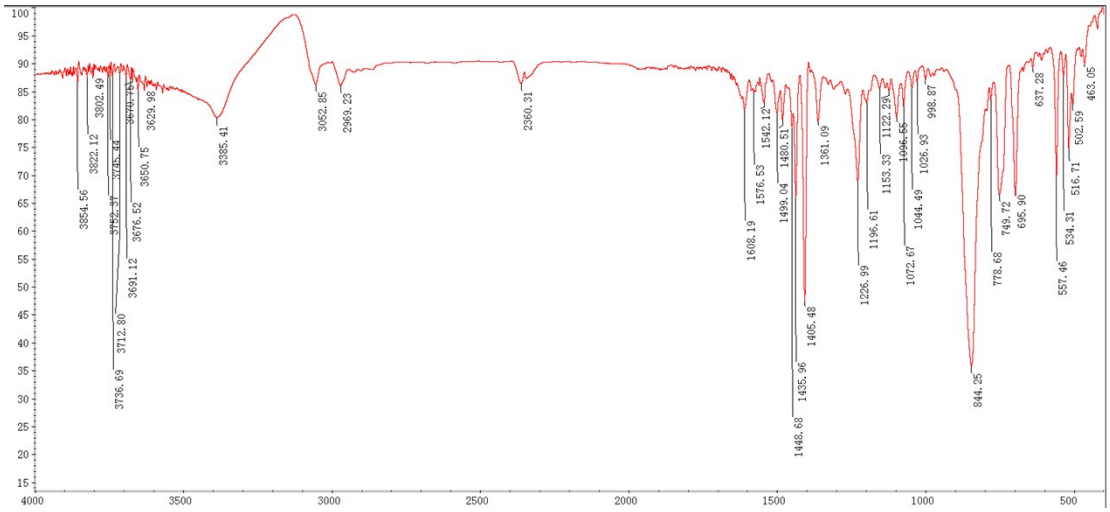

Figure S4. IR spectra of complex **2a**. (*X*-axis: cm⁻¹; *Y*-axis: transmittance).

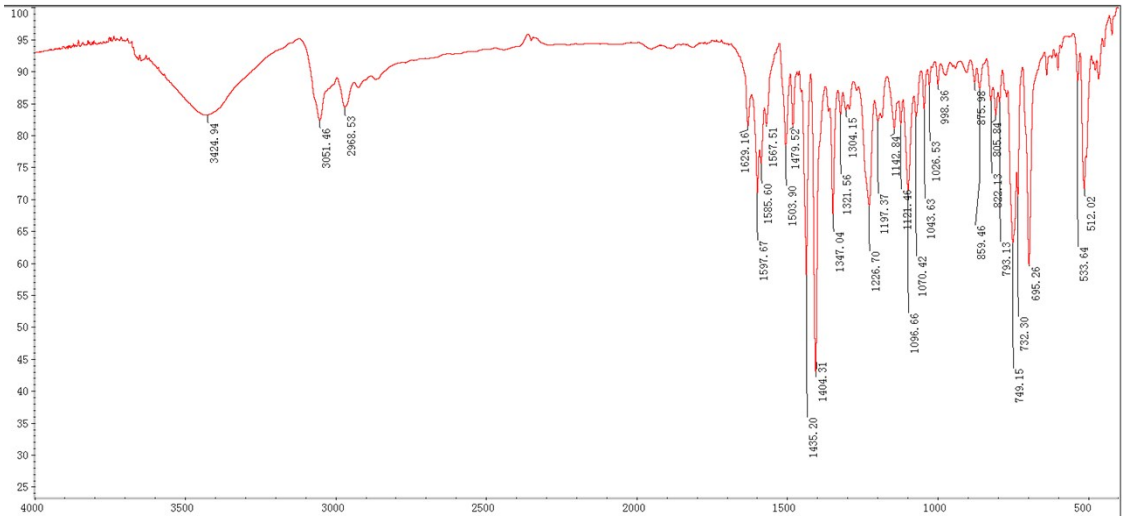

Figure S5. IR spectra of complex **2b**. (*X*-axis: cm⁻¹; *Y*-axis: transmittance).

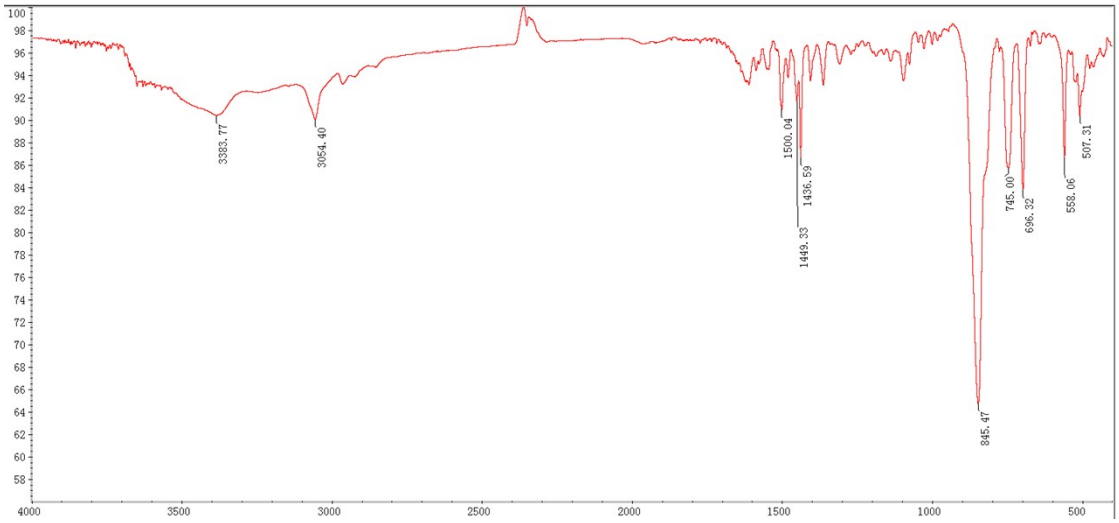

Figure S6. IR spectra of complex **3a**. (*X*-axis: cm⁻¹; *Y*-axis: transmittance).

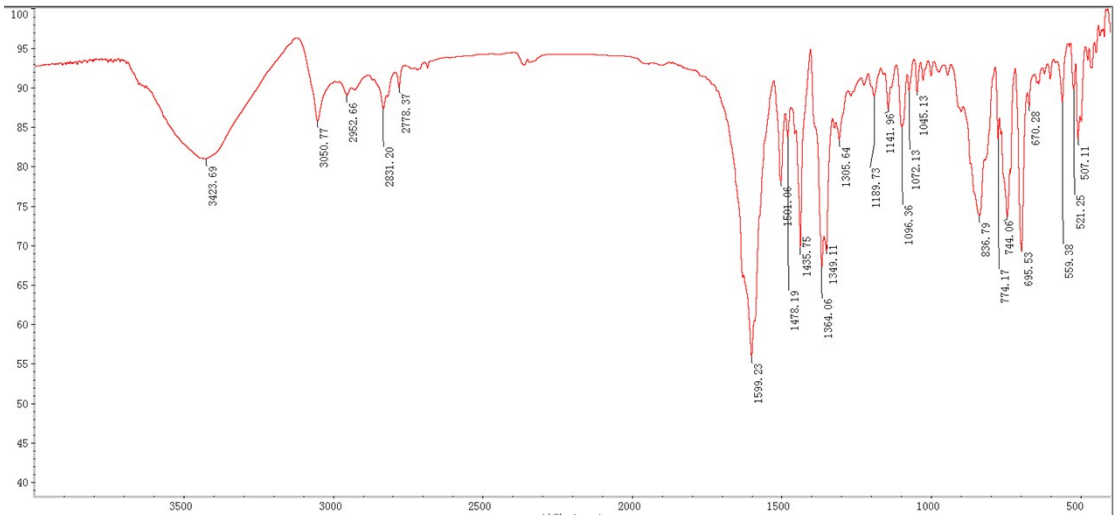

Figure S7. IR spectra of complex **3b**. (*X*-axis: cm⁻¹; *Y*-axis: transmittance).

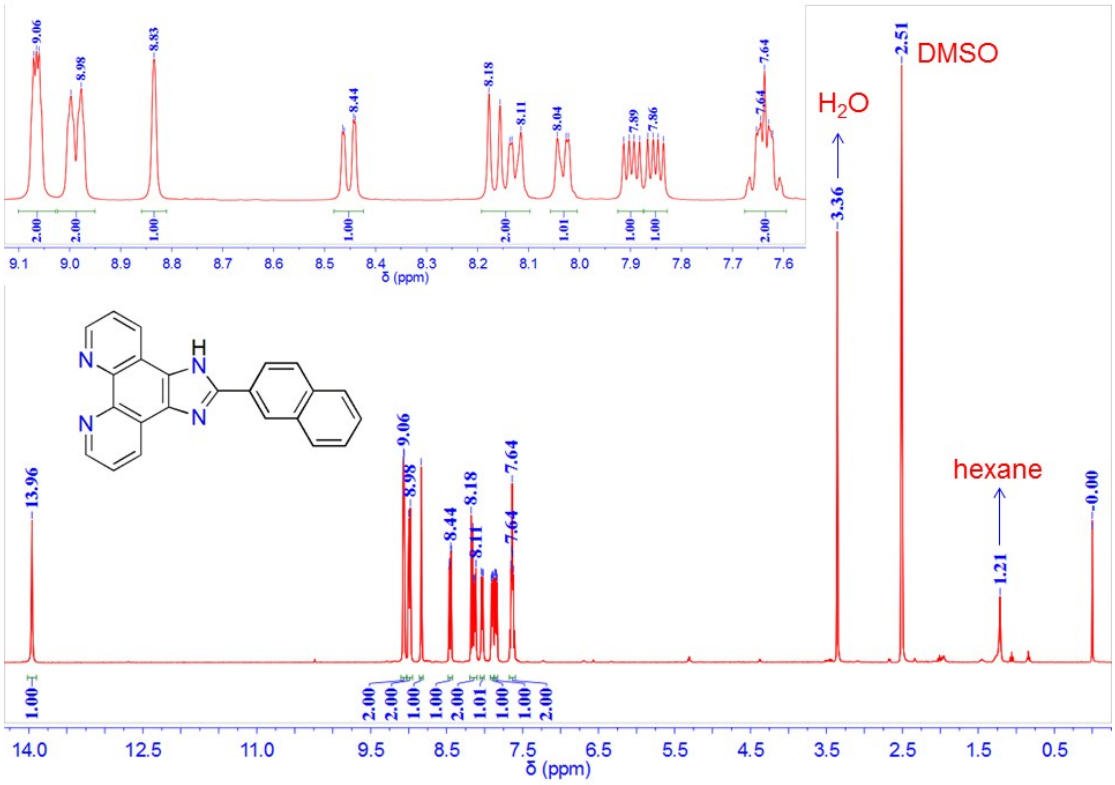

Figure S8. ¹H NMR spectrum of nimpH in DMSO-d_6.

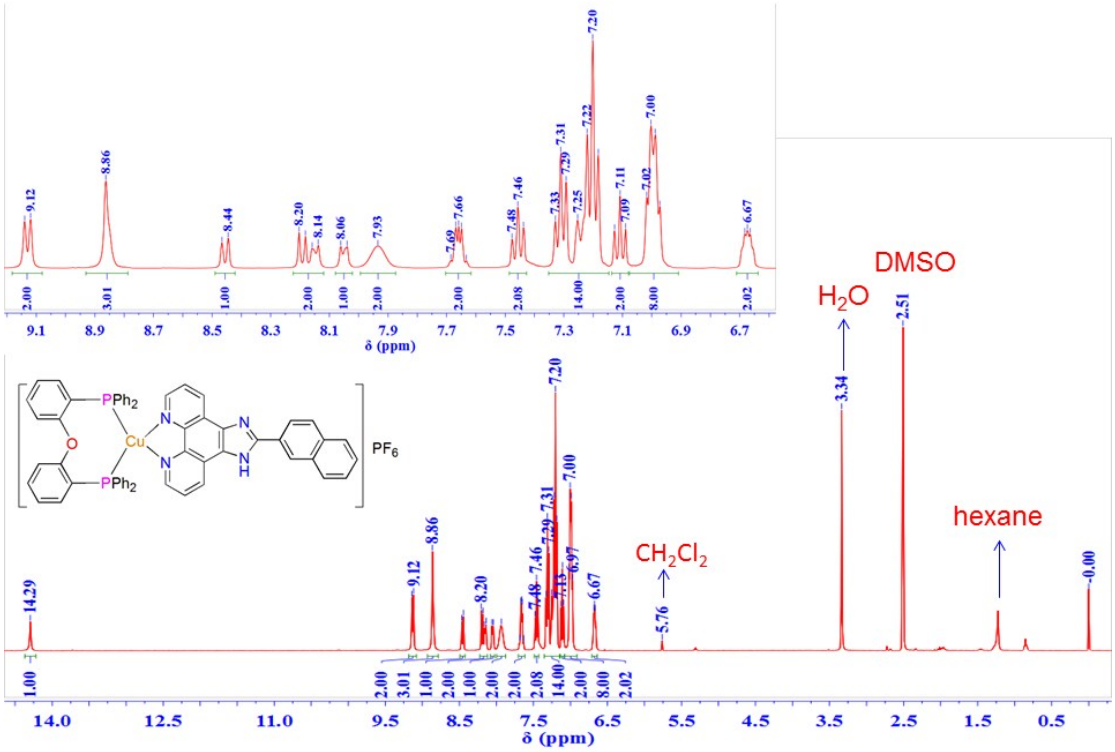

Figure S9. ¹H NMR spectrum of **1a** in DMSO-d_6.

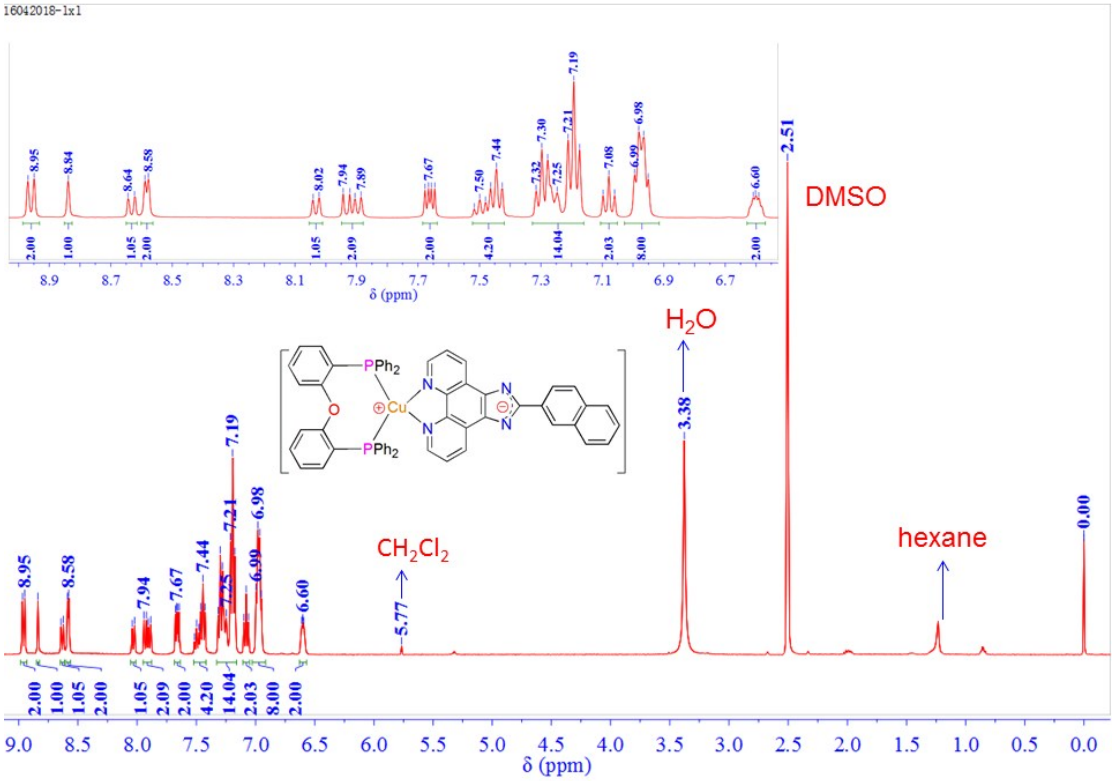

Figure S10. ¹H NMR spectrum of **1b** in DMSO-d_6.

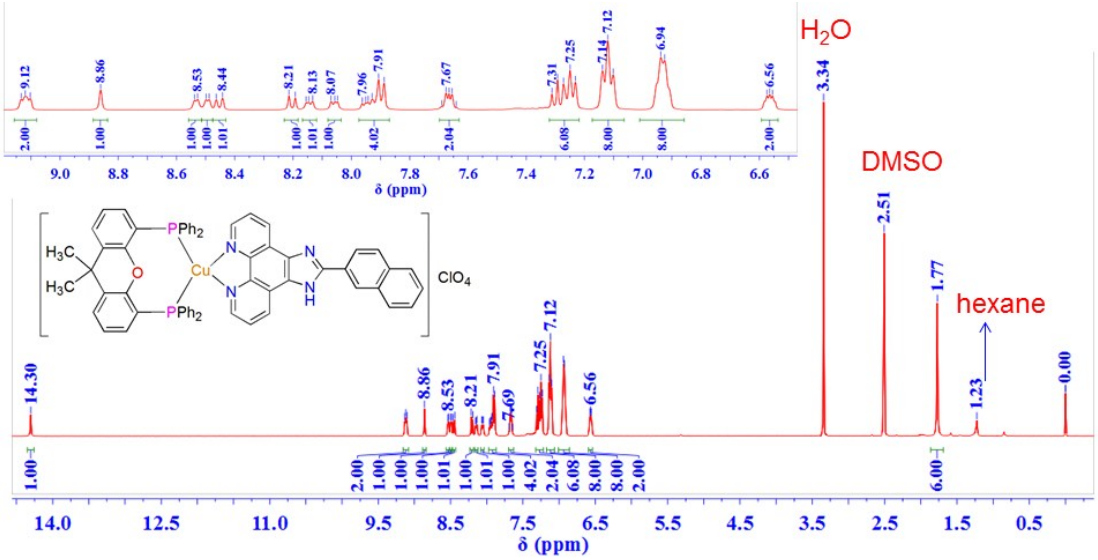

Figure S11. ¹H NMR spectrum of **2a** in DMSO-d_6.

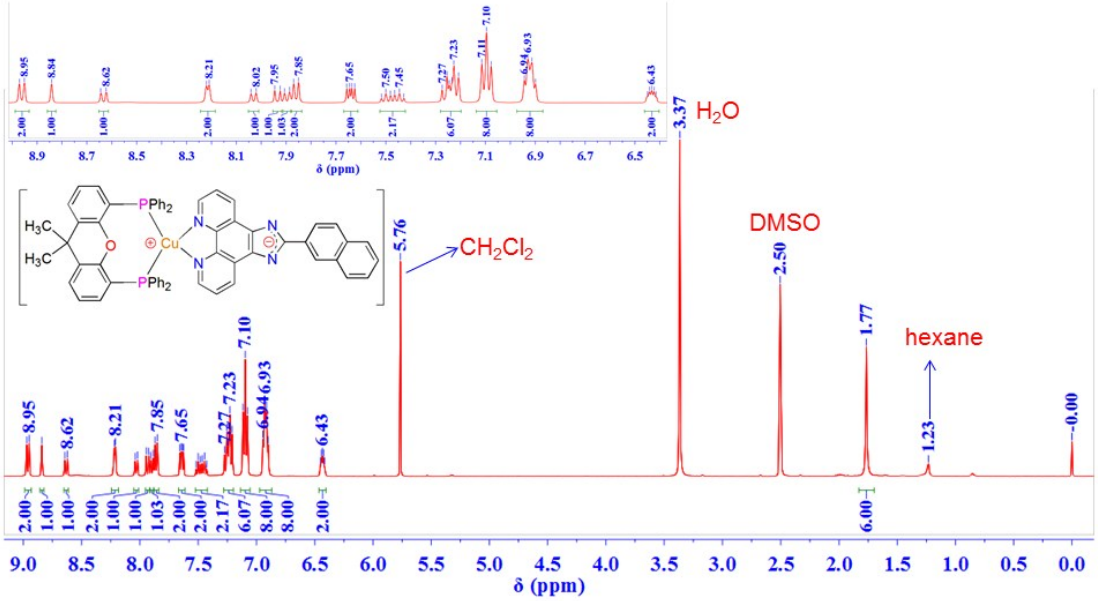

Figure S12. ¹H NMR spectrum of **2b** in DMSO-d_6.

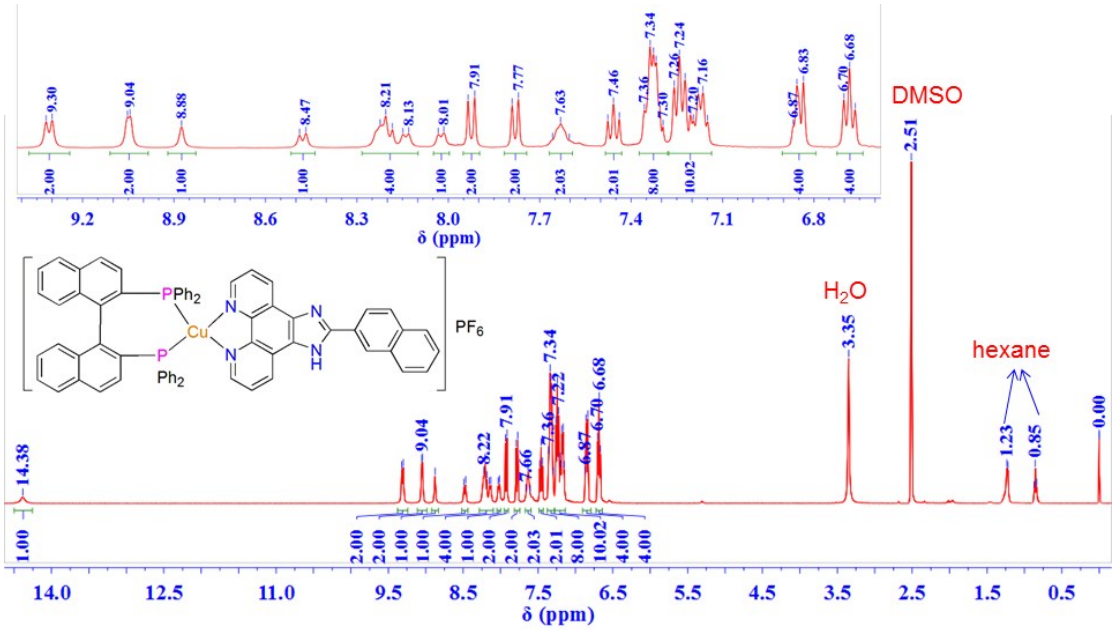

Figure S13. ¹H NMR spectrum of **3a** in DMSO-d_6.

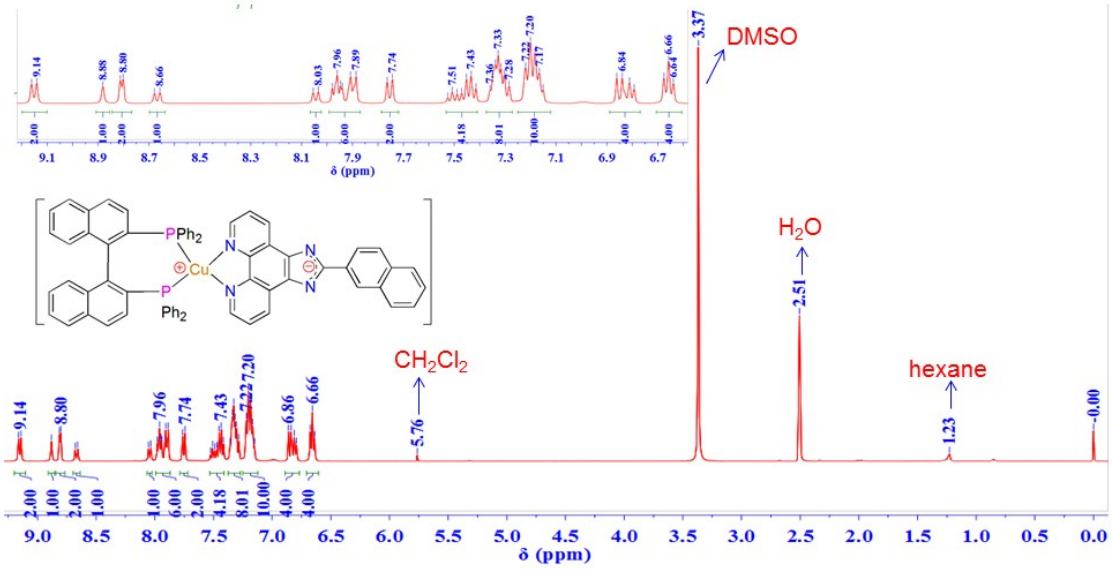

Figure S14. ¹H NMR spectrum of **3b** in DMSO-d_6.

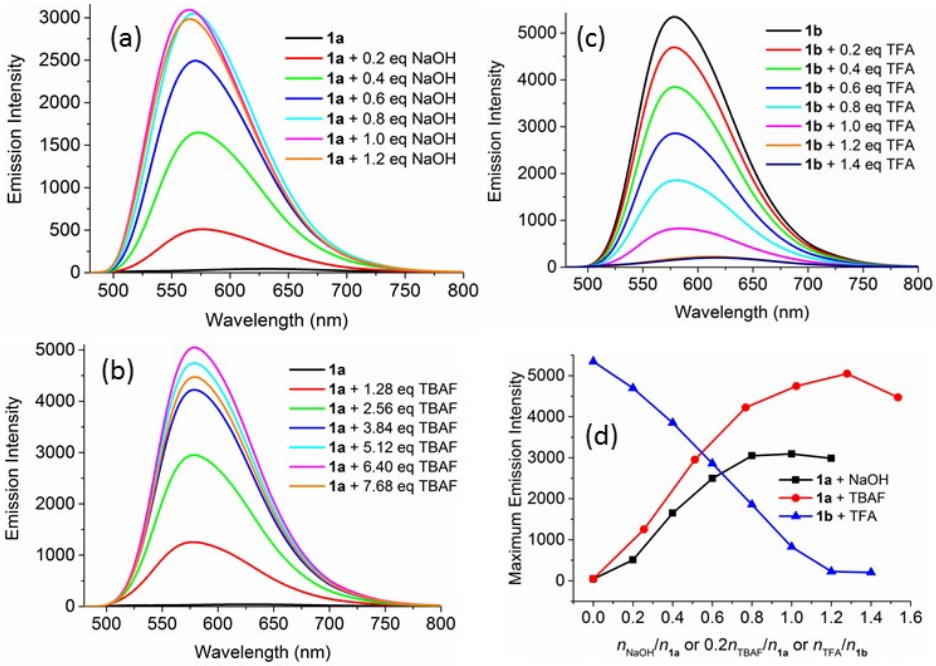

Figure S15. (a) Changes observed in the emission spectra of complex **1a** (2.5×10^{-5} mol·L^{-1}) in DCM upon adding NaOH solution in MeOH (1.0×10^{-3} mol·L^{-1}) at 298 K, (b) Changes observed in the emission spectra of complex **1a** (2.5×10^{-5} mol·L^{-1}) in DCM upon adding TBAF solution in DCM (6.4×10^{-3} mol·L^{-1}) at 298 K, (c) Changes observed in the emission spectra of complex **1b** (2.5×10^{-5} mol·L^{-1}) in DCM upon adding TFA solution in DCM (1.0×10^{-3} mol·L^{-1}) at 298 K and (d) changes of the maximum emission intensity of **1a** and **1b** upon adding different proportions of NaOH, TBAF and TFA.

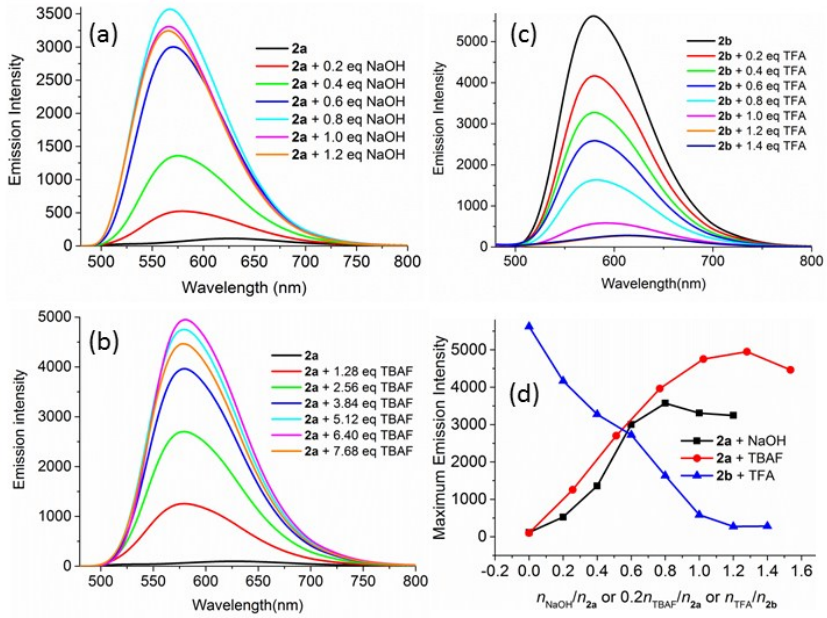

Figure S16. (a) Changes observed in the emission spectra of complex **2a** (2.5×10^{-5} mol·L^{-1}) in DCM upon adding NaOH solution in MeOH (1.0×10^{-3} mol·L^{-1}) at 298 K, (b) Changes observed in the emission spectra of complex **2a** (2.5×10^{-5} mol·L^{-1}) in DCM upon adding TBAF solution in DCM (6.4×10^{-3} mol·L^{-1}) at 298 K, (c) Changes observed in the emission spectra of complex **2b** (2.5×10^{-5} mol·L^{-1}) in DCM upon adding TFA solution in DCM (1.0×10^{-3} mol·L^{-1}) at 298 K and (d) changes of the maximum emission intensity of **2a** and **2b** upon adding different proportions of NaOH, TBAF and TFA.

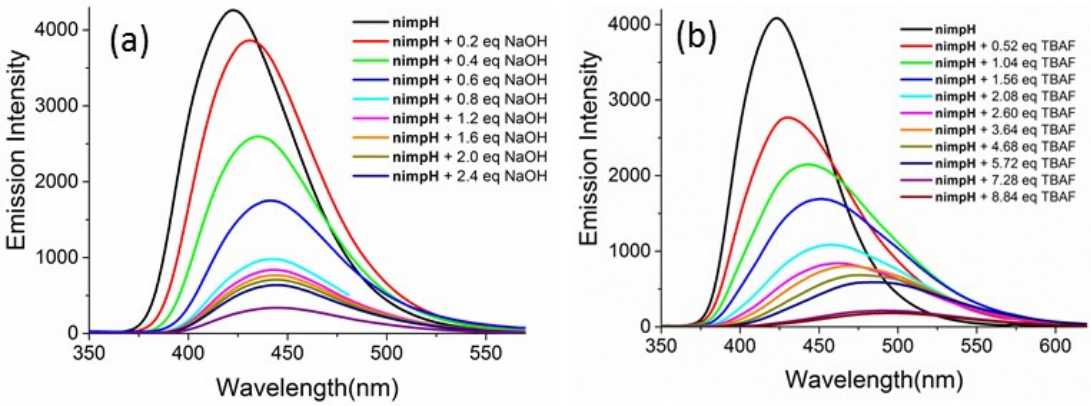

Figure S17. (a) Changes observed in the emission spectra of the free ligand nimpH (2.5×10^{-5} mol·L^{-1}) in DCM upon adding NaOH solution in MeOH (1.0×10^{-3} mol·L^{-1}) at 298 K, (b) Changes observed in the emission spectra of the free ligand nimpH (2.5×10^{-5} mol·L^{-1}) in DCM upon adding TBAF solution in DCM (2.6×10^{-3} mol·L^{-1}) at 298 K. All the emission spectra were obtained upon excitation at 285 nm.

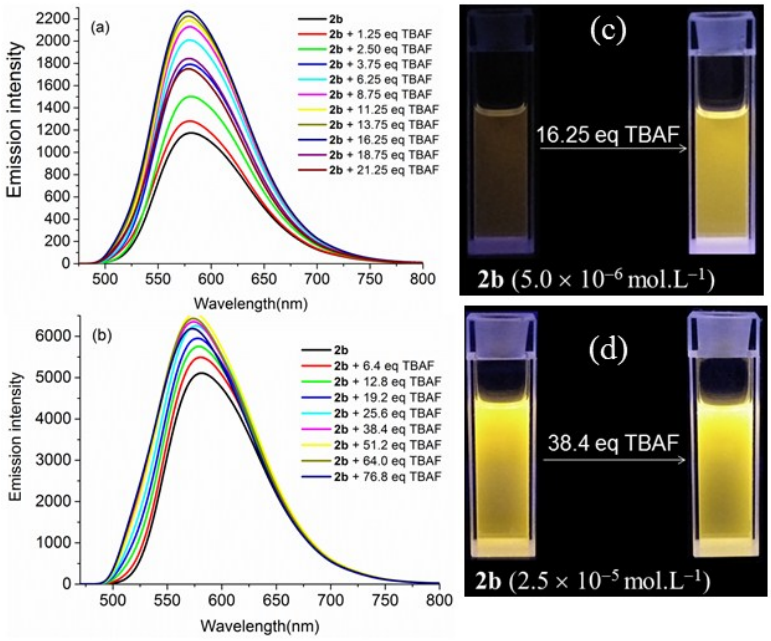

Figure s18. (a) Changes observed in the emission spectra of complex **2b** (5.0×10^{-6} mol·L^{-1}) in DCM upon adding TBAF solution in DCM (1.25×10^{-3} mol·L^{-1}) at 298 K; (b) Changes observed in the emission spectra of complex **2b** (2.5×10^{-5} mol·L^{-1}) in DCM upon adding TBAF solution in DCM (3.20×10^{-2} mol·L^{-1}) at 298 K; (c) and (d) Luminescent images of **2b** radiated with an ultraviolet light at 365 nm before and after addition of TBAF.

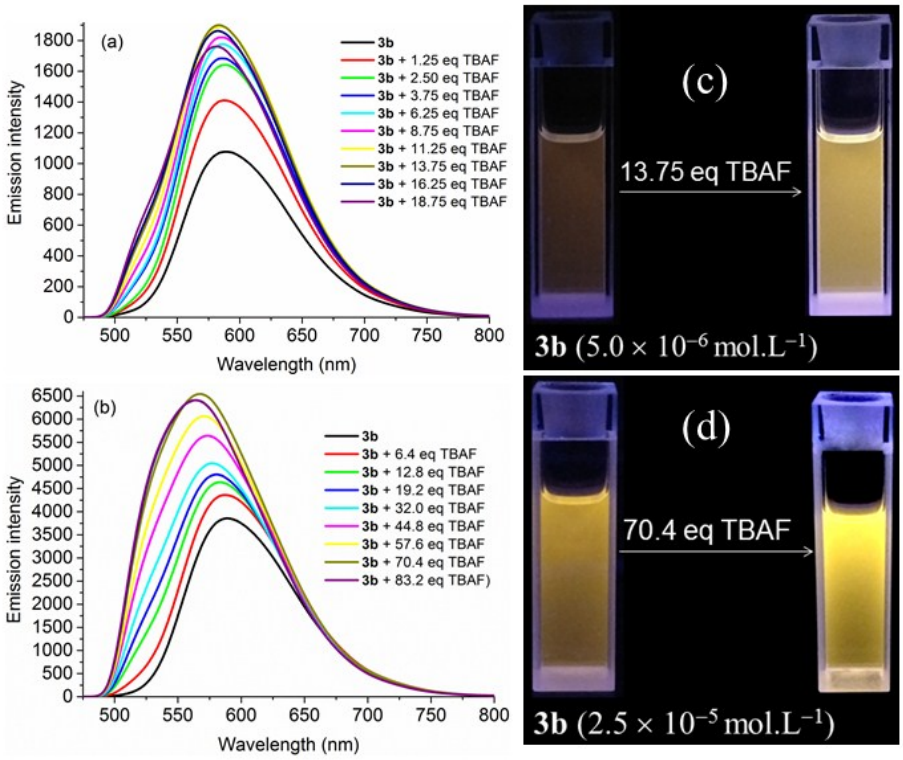

Figure s19 (a) Changes observed in the emission spectra of complex **3b** (5.0×10^{-6} mol·L⁻¹) in DCM upon adding TBAF solution in DCM (1.25×10^{-3} mol·L⁻¹) at 298 K; (b) Changes observed in the emission spectra of complex **3b** (2.5×10^{-5} mol·L⁻¹) in DCM upon adding TBAF solution in DCM (3.20×10^{-2} mol·L⁻¹) at 298 K; (c) and (d) Luminescent images of **3b** radiated with an ultraviolet light at 365 nm before and after addition of TBAF.

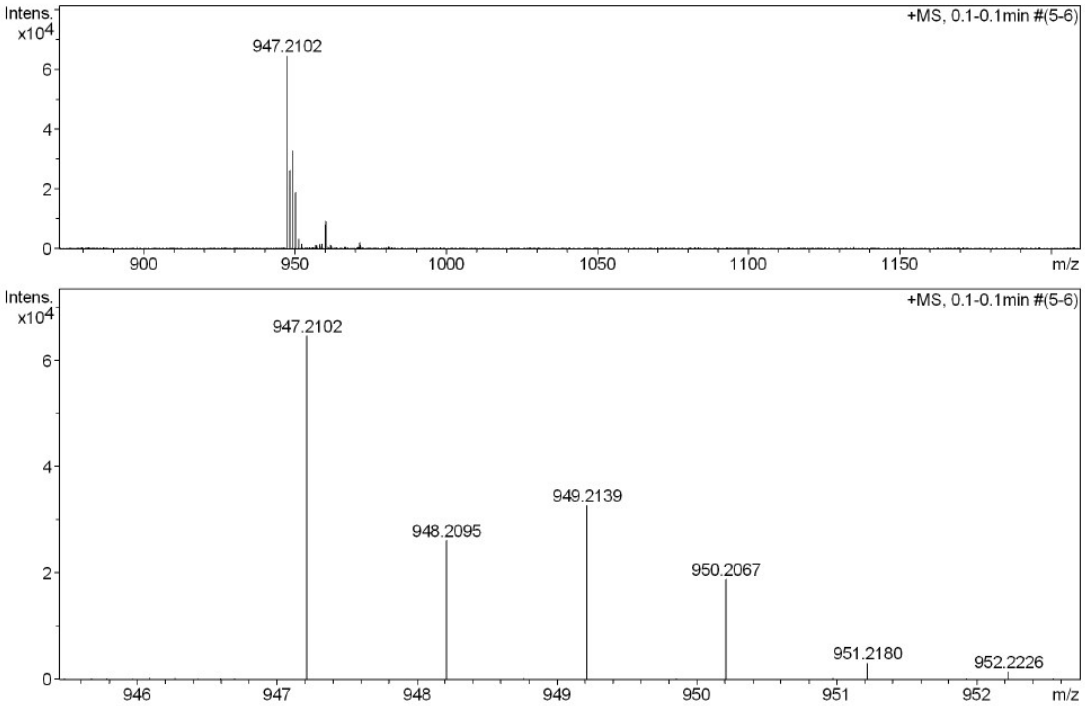

Figure S20. ESI-MS spectra of complex **1a** with collision cell energy at 10 ev.

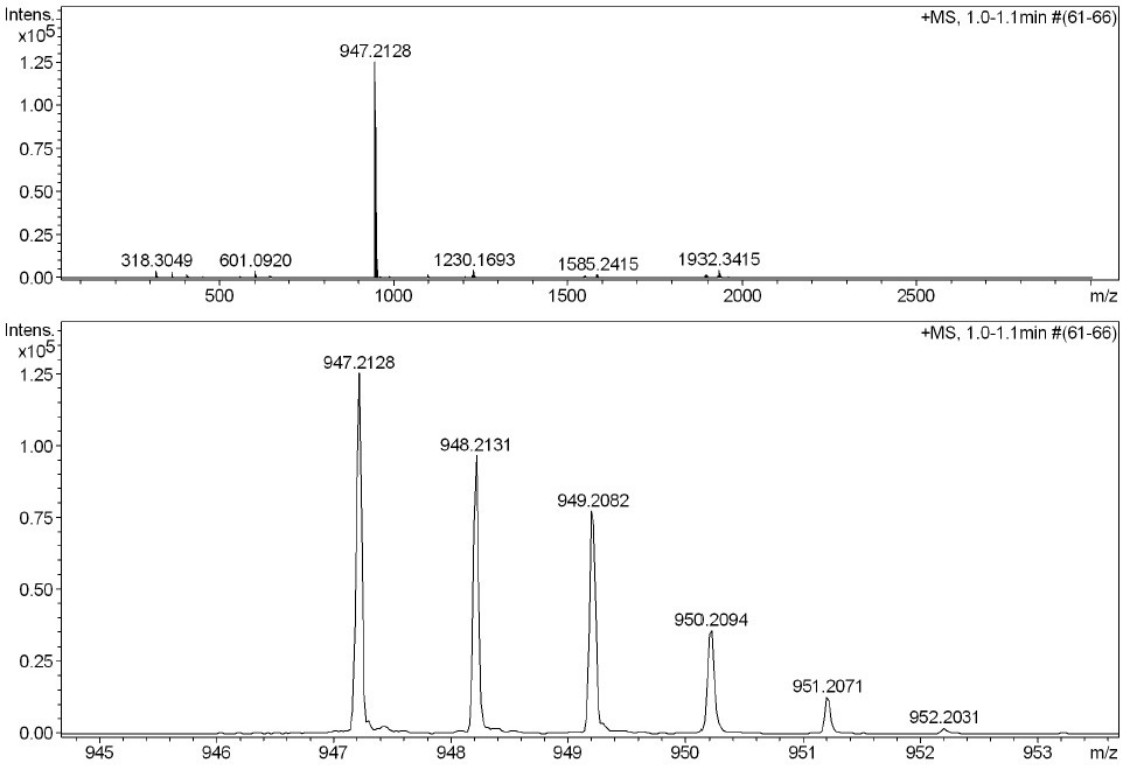

Figure S21. ESI-MS spectra of complex **1b** with collision cell energy at 10 ev.

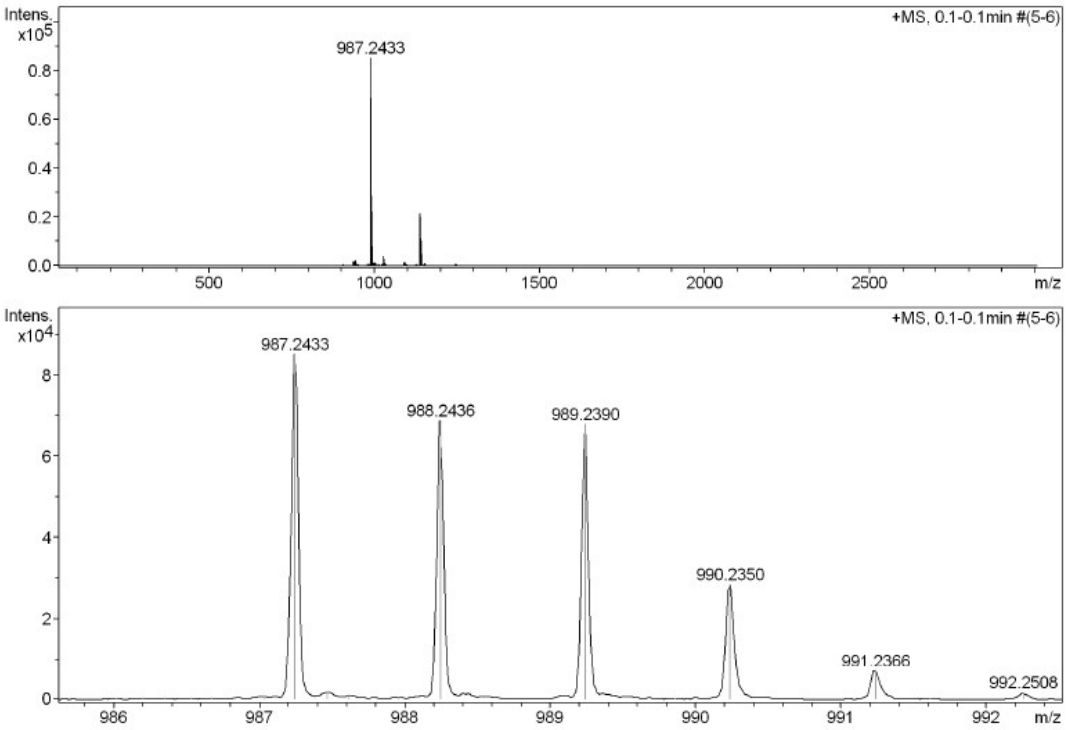

Figure S22. ESI-MS spectra of complex **2a** with collision cell energy at 10 ev.

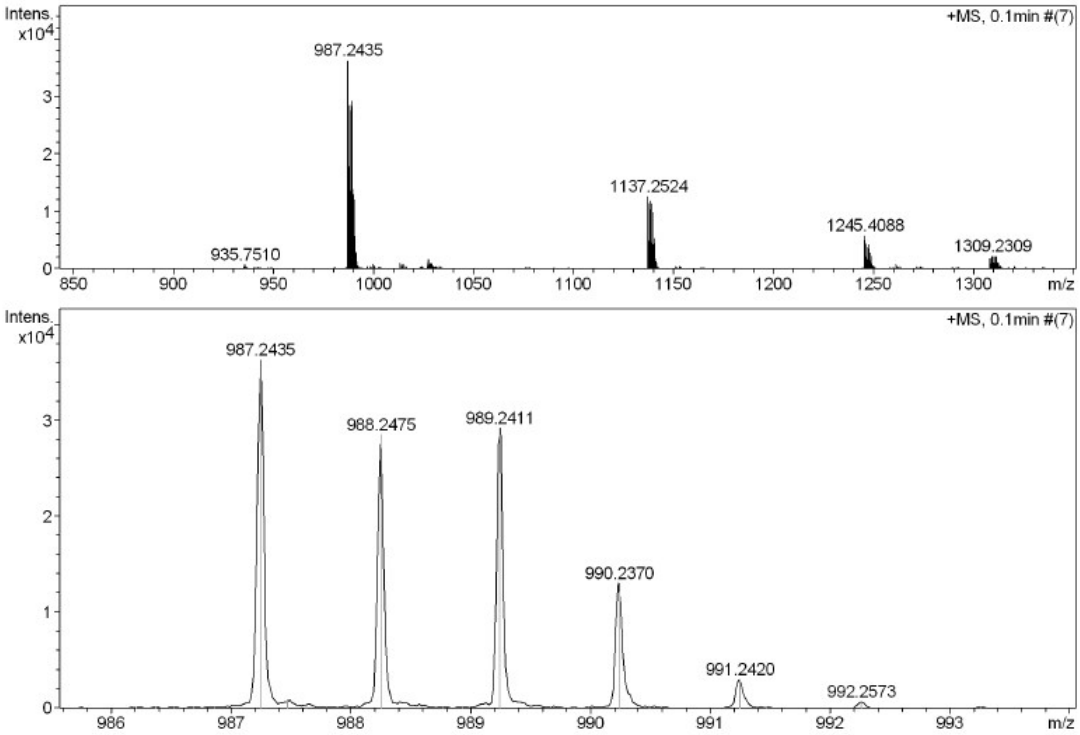

Figure S23. ESI-MS spectra of complex **2b** with collision cell energy at 10 ev.

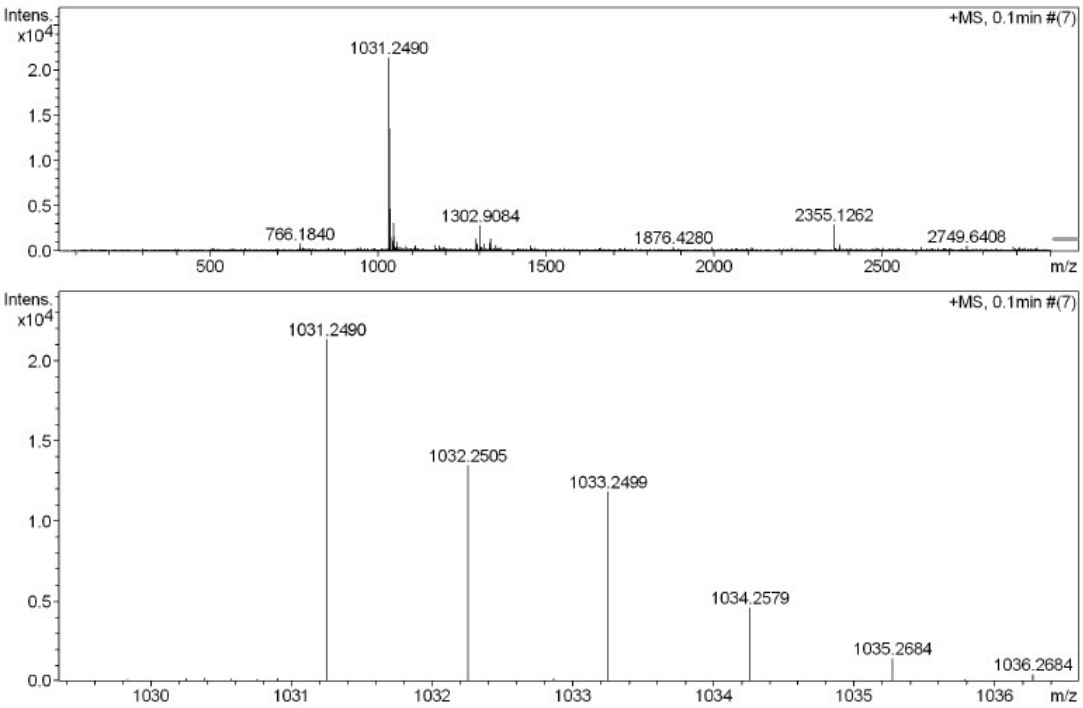

Figure S24. ESI-MS spectra of complex **3a** with collision cell energy at 10 ev.

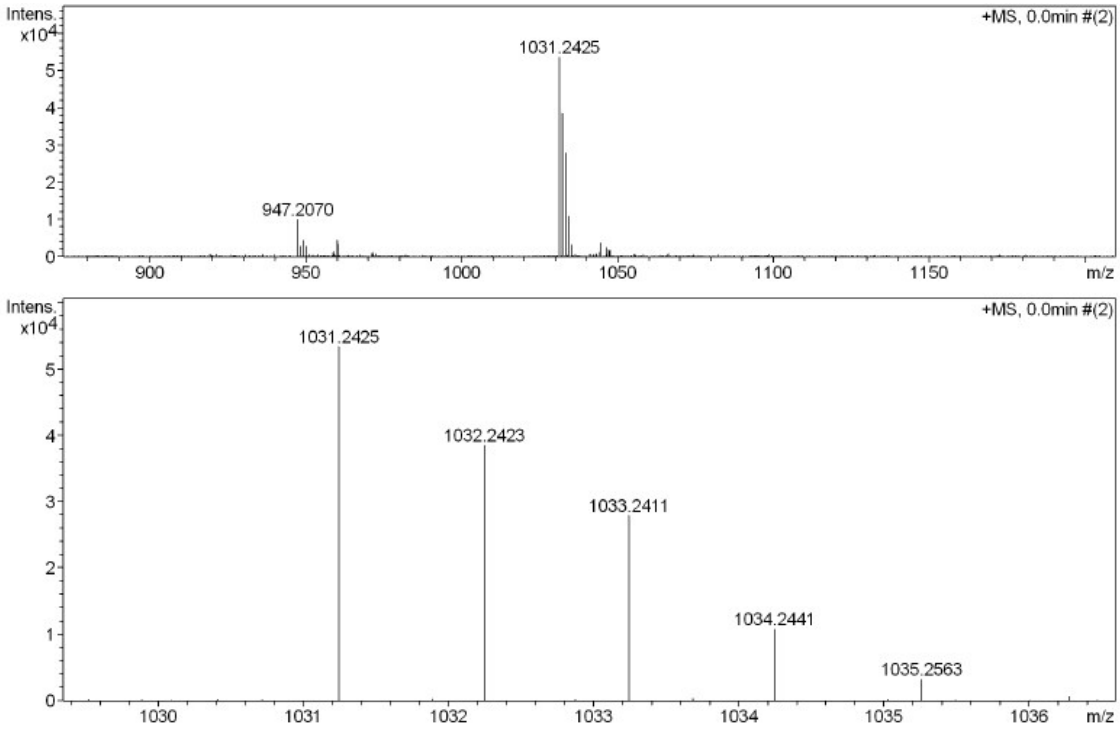

Figure S25. ESI-MS spectra of complex **3b** with collision cell energy at 10 ev.

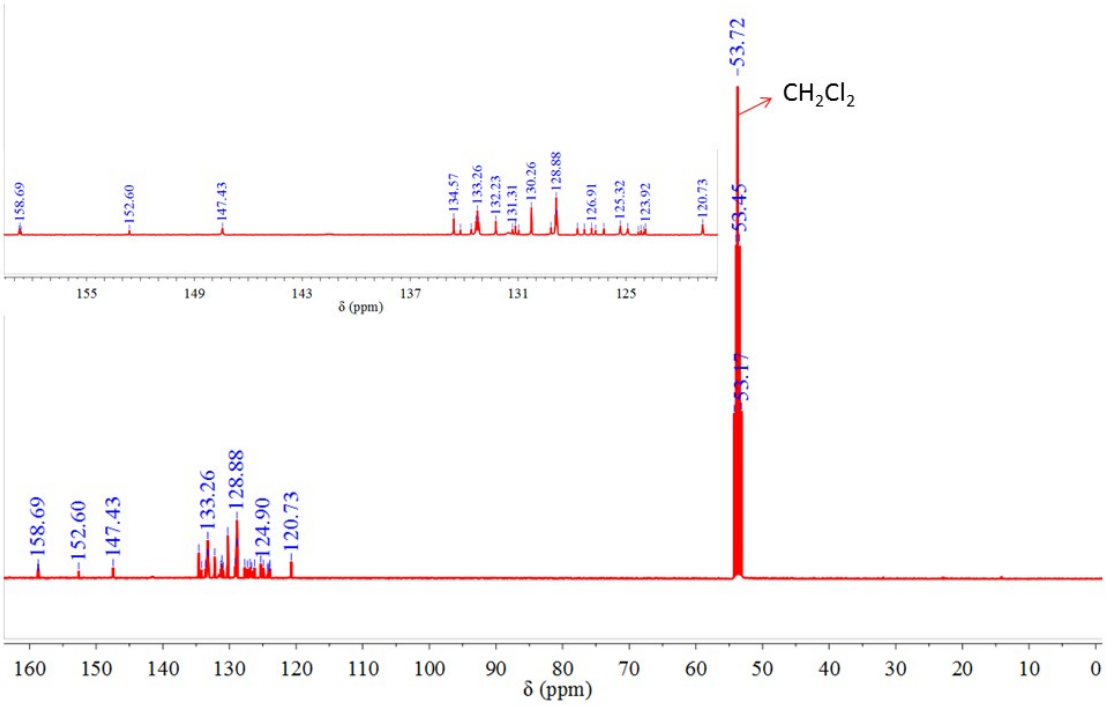

Figure S26. ^{13}C NMR spectrum of **1a** in CD_2Cl_2.

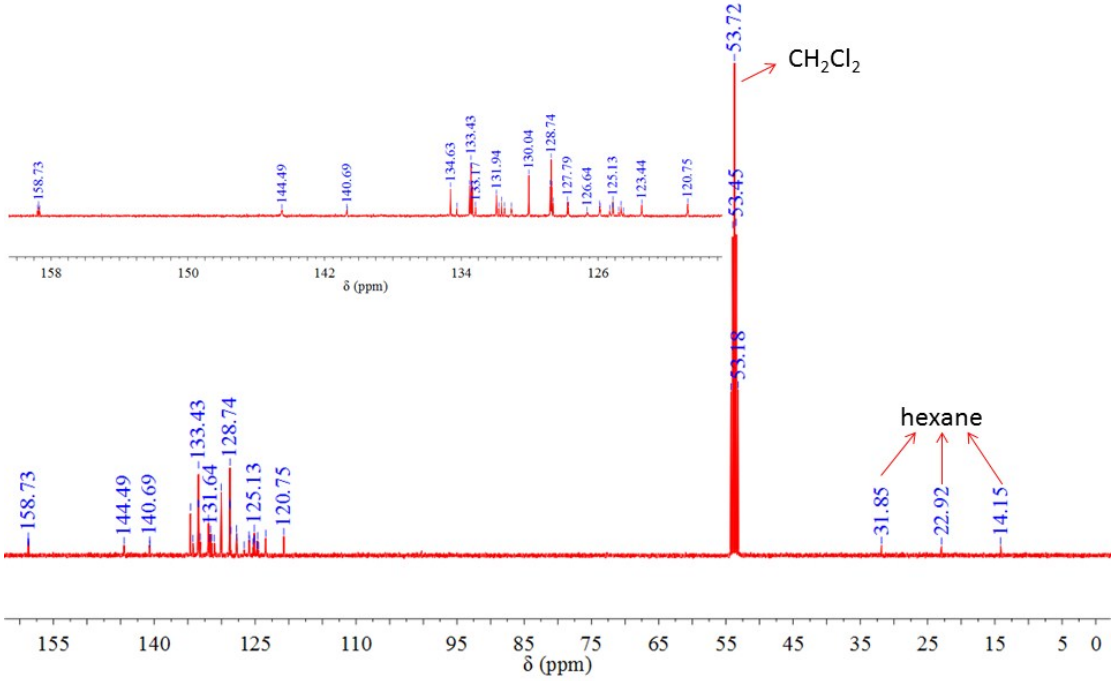

Figure S27. ^{13}C NMR spectrum of **1b** in CD_2Cl_2.

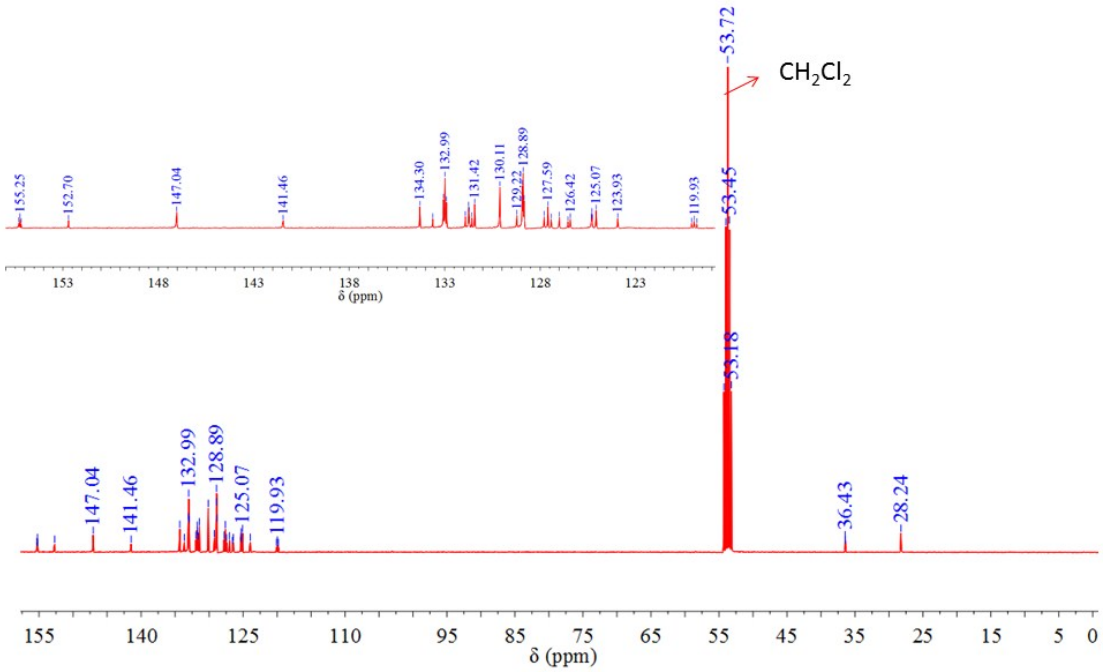

Figure S28. ^{13}C NMR spectrum of **2a** in CD_2Cl_2.

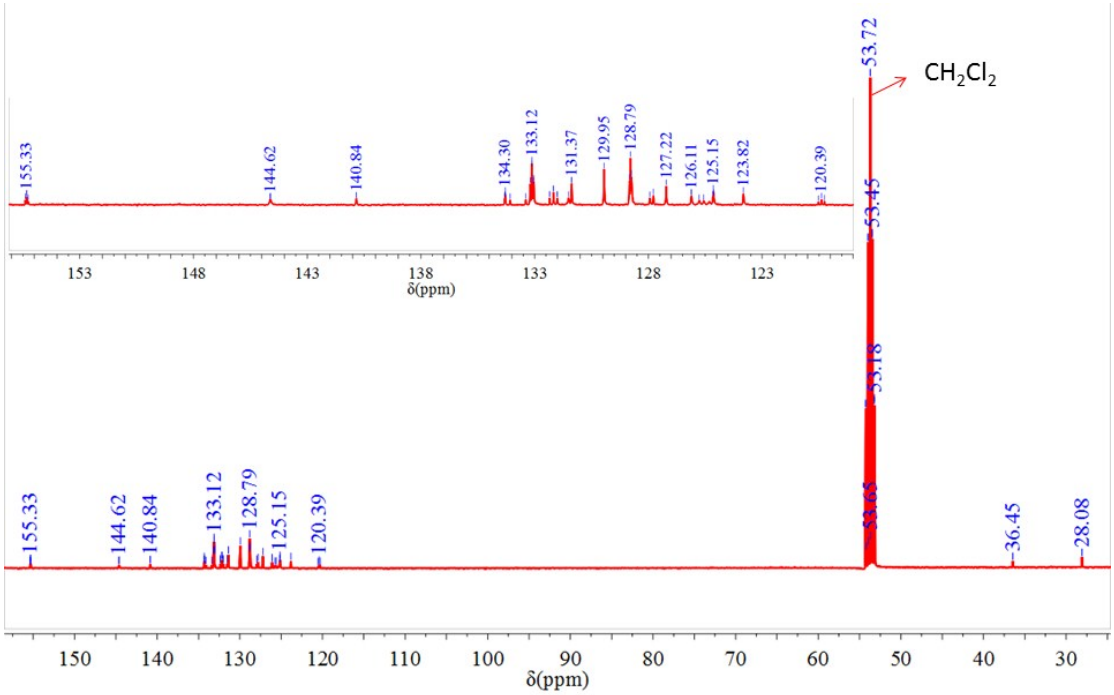

Figure S29. ^{13}C NMR spectrum of **2b** in CD_2Cl_2.

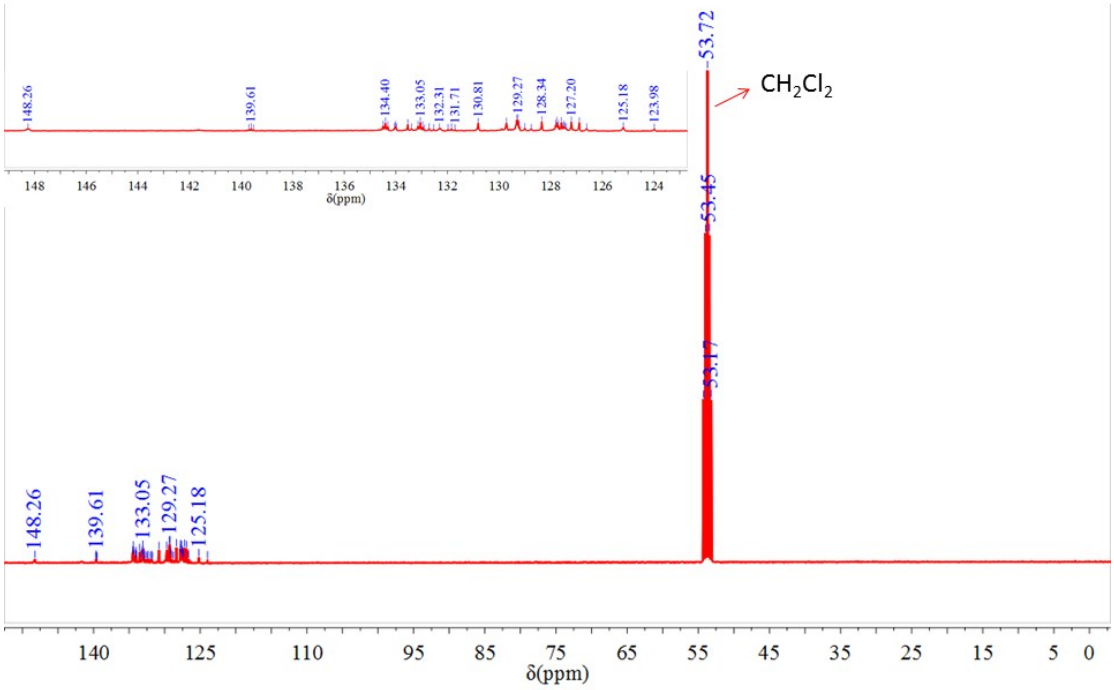

Figure S30. ^{13}C NMR spectrum of **3a** in CD_2Cl_2.

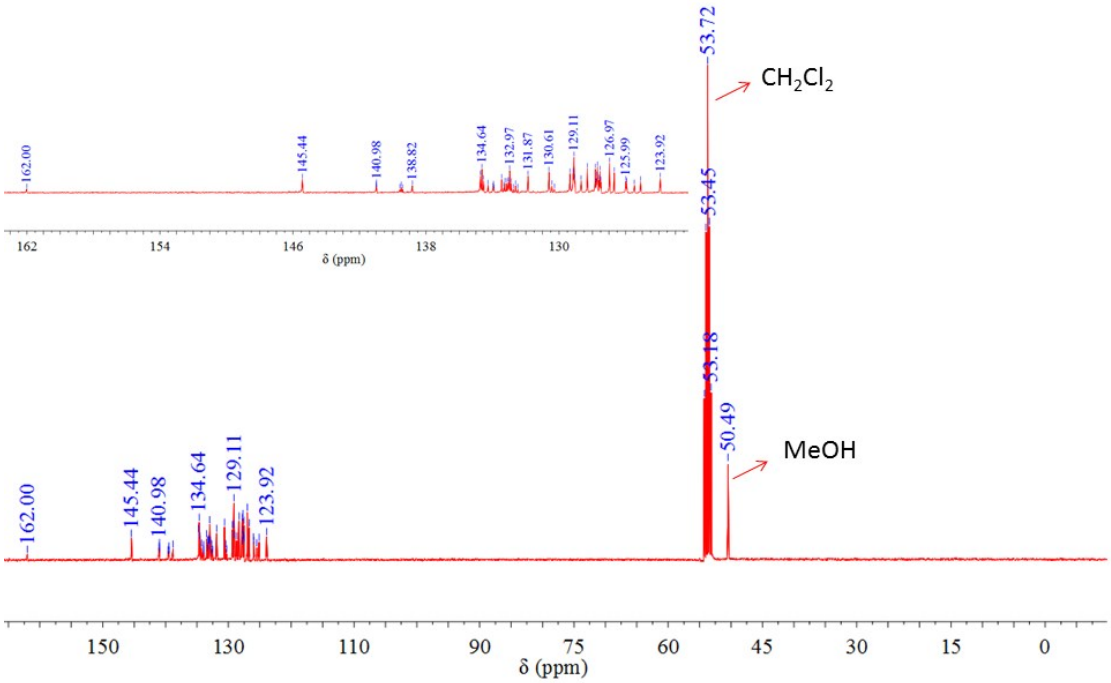

Figure S31. ^{13}C NMR spectrum of **3b** in CD_2Cl_2.